THE POTENTIAL OF USING SENTINEL-2 SATELLITE IMAGERY IN ASSESSING BACTERIAL LEAF BLIGHT ON RICE IN WEST JAVA, INDONESIA

Oliver Caasi[1,5], Chiharu Hongo[2], Suryo Wiyono[3], Yuti Giamerti[4,6], Daiki Saito[4], Koki Homma[4], and Masahiro Shishido[1, *]

[1]Graduate School of Horticulture, Chiba University, 648 Matsudo, Matsudo-shi, Chiba 271-8510, Japan

[2]Center for Environmental Remote Sensing, Chiba University, 1-33 Yayoi-cho, Inage-ku, Chiba-shi, Chiba 263-8522, Japan

[3]Department of Plant Protection, Bogor Agricultural University, Jln. Meranti Kampus IPB Darmaga, Bogor 16680, Indonesia

[4]Graduate School of Agricultural Science, Tohoku University, 468-1 Aramaki Aza Aoba, Aoba-ku, Sendai, Miyagi 980-8572, Japan

[5]Pangasinan State University, Sta. Maria, Pangasinan 2440, Philippines

[6]Banten Assessment Institute for Agricultural Technology Indonesian Ministry of Agriculture, Ciruas Serang, Banten 42182, Indonesia

*Corresponding author: shishido@faculty.chiba-u.jp

(Received: September 29, 2019; Accepted: March 23, 2020)

ABSTRACT

Bacterial leaf blight (BLB) caused by *Xanthomonas oryzae* pv. *oryzae* has affected rice production in tropical to sub-tropical countries. In Indonesia, it is one of the most important diseases of rice. This study sought to develop an inexpensive and accurate method of assessing BLB damage using remote sensing technology. The field assessments were conducted in Cianjur, West Java, Indonesia in 2017 and 2018. Visual assessments of disease severities were scored, and GPS coordinates of each sample plot were recorded. The potential of using spectral data from earth-observing Sentinel-2 satellites was explored in detecting BLB damages. Correlations between BLB severities and spectral indices proposed in related studies were evaluated, revealing that all bands of Sentinel-2A except Band 10 can potentially be useful for BLB damage detection. The visible, red-edge, near-infrared, and shortwave infrared regions may be usable for discriminating healthy rice plants from BLB damaged plants. BLB severities were strongly correlated with spectral index values, and four indices, BLB Index 1, Green Red Edge index, and Disease-Water Stress indices 1 and 2, in addition to two common vegetation indices of Normalized Difference Vegetation Index and Ratio Vegetation Index, were practically applicable for estimating the BLB severities.

Key words: *Xanthomonas oryzae* pv. *oryzae*, disease severity, remote sensing

INTRODUCTION

Bacterial leaf blight (BLB), caused by *Xanthomonas oryzae* pv. *oryzae*, is one the most common diseases of rice in the tropical to subtropical zones worldwide, especially in Asia, causing significant losses to key production areas (IRRI 2017; Mew et al. 1993; Swings et al. 1990). BLB symptoms first appear as chlorosis at the leaf tips then wavy yellow to brown lesions progress toward the leaf base which eventually turn greyish-white (IRRI 2017). Field patches infested with bacterial blight have a whitish, ragged appearance. In Indonesia, BLB was first observed in 1948-49 in Bogor, West Java and was called "kresek" (Reitsma and Schure 1950). It is now considered as a threat to Indonesian rice production (FAO 2019). In 2008, 3.87% of annual rice production in Indonesia or approximately 2.33 million metric tons was lost due to flood, drought, pests, and diseases (Pasaribu,

2010). To protect the farmers from these risks, a new Indonesian law was passed in 2013, called Farmer Protection and Empowerment Act to implement crop insurance nationwide (Pasaribu 2016). BLB is one of the main causes of crop loss listed for crop insurance indemnity claims in Indonesia (FAO 2019). Farmers could make an insurance claim only if the damage intensity reached level of 75% or above; and the extent of damage reaches minimum 75% of total area of the insured crop (Pasaribu 2016). Pest observers are tasked to monitor the incidence and severity of pest and disease damages to facilitate crop insurance claims. Pest monitoring sometimes only cover limited area and estimating the extent of damage over large rice production areas may not be possible or would be very time consuming. In Indonesia, many rice paddies are small and contiguous in communities that are not readily accessible due to the rugged terrain and limited road networks. This situation has made disease and pest observation and assessment even more challenging. Hence, remote sensing technology may be considered as one of the components of damage monitoring for crop insurance policy claims and risk assessment strategy formulation (Gogoi et al. 2018; Martinelli et al. 2015). Utilization and adoption rate of remote sensing technology with either multispectral or hyperspectral imagery for agriculture and environmental management has been increasing (Cordova et al. 2012; George 2000; Haack and Ryerson 2016).

In crop production, remote sensing involves measurement of reflectance of electromagnetic radiation from vegetation area in the visible (390 to 770 nm), near-infrared (NIR, 770 to 1300 nm) or middle-infrared (1300 to 2500 nm) regions (Mahlein et al. 2013; Reynolds et al. 2012). In remote sensing, surface reflectance values from satellite or airborne imagery are extracted and correlated to ground truth data (Calderon et al. 2013; Reynolds et al. 2012). Relevant broad bands or specific wavelengths can be selected for spatial pattern generation, followed by computing spectral or vegetation indices. Such indices have been used for estimating chlorophyll content, canopy density and leaf area index as well as detecting plant diseases at canopy, field, and regional scale (Apan et al. 2010; Calderon et al. 2013; Mahlein et al. 2013; Mirik et al. 2011; Reynolds et al. 2012; Singh et al. 2012; Yang 2010). Hongo et al. (2015) developed a damage assessment method of rice crop for agricultural insurance using SPOT (*Satellite Pour l' Observation de la Terre*) 5 satellite data. Other satellite products also detect BLB damage such as Indian Remote Sensing Satellite with Linear Imaging and Self Scanning sensor (LISS IV) (Das et al. 2015) and RapidEye Satellite (Berlin, Germany) (Hongo et al. 2017). Canopy-level measurements of hyperspectral reflectance from rice plants affected by BLB were also conducted (Hongo et al. 2017; Singh et al. 2012; Yang 2010;).

In this study, we attempted to detect BLB using Sentinel-2 satellite products (European Space Agency, ESA, Frascati, Italy). Sentinel-2 is designed to provide open access multispectral images that can be processed to distinguish between different crop types as well as data on leaf area index, leaf chlorophyll content and leaf water content for accurate monitoring of plant growth (ESA 2019). We aimed at developing an inexpensive and accurate method of assessing BLB severity using Sentinel-2 Multispectral Instrument (MSI) satellite imagery by searching the most relevant band as well as spectral indices, and by surveying rice paddies with BLB incidence. This is the first study to use Sentinel-2 satellite data in discriminating different levels of BLB severity.

MATERIALS AND METHODS

Field assessment. The field assessment was conducted in Cianjur, West Java Province, Indonesia, 29 July–3 August, 2017 and 24–27 September, 2018. Site selection was done with the assistance from the local pest observers and rice farmer coordinators. A total of six sites in 2017 and four sites in 2018 (Fig. 1) were identified as main sampling sites which represented the rice producing villages in the locality. Rice paddies with different levels of BLB severity from flowering to ripening stage were sampled. In each site, sampling on contiguous rice fields were conducted with the assistance from an experienced pest observer using sampling method described by Delp et al. (1986). In 2017, single rice-hills were sampled across paddy field diagonally with a total of 10 rice-hills per sampling area. The 10 rice-hills

per paddy field were grouped as one cluster. Each sampling area is approximately 30 m across. In 2018, 3 rice-hills per 1 m^2 sample plot were randomly selected across the paddy field. Five sample plots or a total 15 rice-hills per paddy field were grouped as one cluster. Geographical coordinates of the sampled rice-hills were recorded using Garmin eTrex 30xJ (GPS) device (Olathe, Kansas, USA).

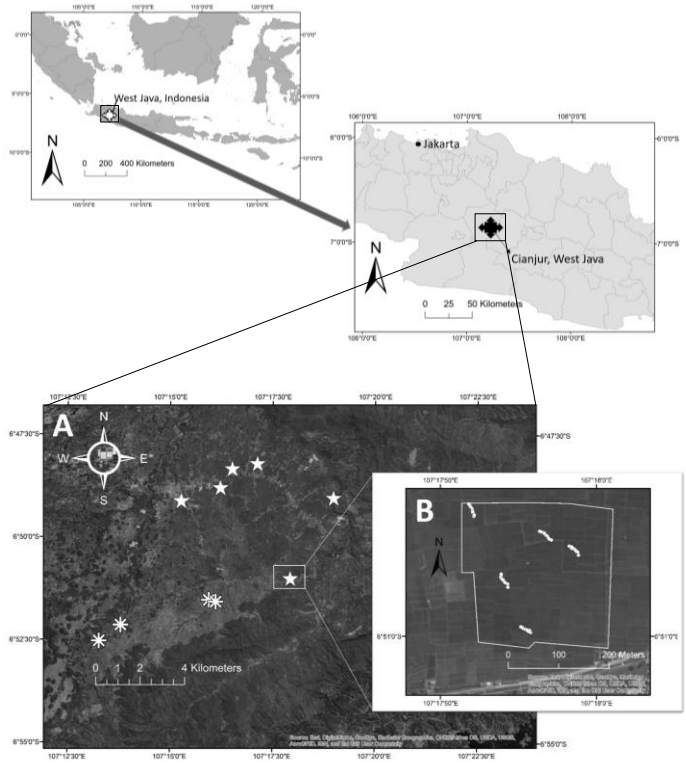

Fig. 1. Location of the field assessments (inset a) conducted in Cianjur, West Java, Indonesia in 2017 (★) and 2018 (*). Actual geospatial position (inset b) of sample plots across rice paddy fields in Sukatani (Location 1) are shown in white dots.

The disease severity of BLB was determined by estimating the percentage of infected surface area of rice leaves, and scored each hill based on the manual released by the Indonesian Crop Protection Bureau. For BLB, a scale of 0 to 9 was adopted and rice-hills were scored based on the size of lesion according to the followings, 0: no lesions observed; 1: >0 to 5%; 3: >5 to 25%; 5: >25% to 50%; 7: >50% to 75%; and 9: >75%. The following formula was used for computing the disease severity index per sample plot or paddy field:

Disease severity index (DSI) = Σ[(number of rice-hills at the scale)/(total number of hills x 9)] × 100

Satellite data acquisition. Multi-spectral images from Sentinel-2A satellite acquired on July 24, 2017 and September 27, 2018 were downloaded from the US Geological Survey website as open access products using the Earth Explorer platform (USGS, Reston, Virginia, USA). These are the products acquired with least clouds and closest to the field survey dates. Since only Sentinel-2A satellite data products were used in this study, satellite bands discussed herein are all Sentinel-2A as shown in Table 1. Sentinel-2B satellite flight dates did not coincide with the dates of field assessments.

Table 1. Description of multi-spectral instrument (MSI) sensors of the Sentinel-2A[a]

Sentinel-2A Band name	Central wavelength (nm)	Bandwidth (nm)	Resolution (m)
B1 - Coastal aerosol	442.7	21	60
B2 - Blue	492.4	66	10
B3 - Green	569.8	36	10
B4 - Red	664.6	31	10
B5 - Vegetation Red Edge	704.5	15	20
B6 - Vegetation Red Edge	740.5	15	20
B7 - Vegetation Red Edge	782.8	20	20
B8 - Near-infrared	832.8	106	10
B8A - Near-infrared (narrow)	864.7	21	20
B9 - Water vapor	945.1	20	60
B10 - Shortwave Infrared-Cirrus	1373.5	31	60
B11 - Shortwave Infrared	1613.7	91	20
B12 - Shortwave Infrared	2202.4	175	20

[a] Source: ESA (2019)

Satellite product processing. Sentinel Application Platform (SNAP version 6.0.5), a GIS program developed by the European Space Agency for Sentinel data processing, was used in atmospheric correction, vegetation indices computation and band combination. The ArcMap (version 10.5, ESRI, California, USA), a main component of ArcGIS developed by Environmental Systems Research Institute (ESRI), was used in viewing multi-spectral images and index maps and extracting geospatial data. ArcMap was also used in generating geographic information system (GIS) maps showing BLB spatial pattern.

Atmospheric correction. The Sentinel-2A images were pre-processed for atmospheric correction using the Sentinel-2 Atmospheric Correction (Sen2Cor) Processor (ver. 255, ESA, Frascati, Italy) in the SNAP toolbox (ver. 6.0.5, ESA, Frascati, Italy). This process includes the conversion of Top-of-Atmosphere (TOA) reflectance (Level-1C image) to Bottom-of-Atmosphere (BOA) or surface reflectance, a Level-2A output (ESA, 2018; Louis et al. 2016). Surface reflectance is the measure of reflectance on the surface of the ground whereas Top-of-Atmosphere (TOA) reflectance is the measure of reflectance at the sensor. Correction process removes atmospheric distortions. Sen2Cor also performs the terrain and cirrus correction. Sen2cor parameters was set to '0' ozone content (default for auto), 'Auto' for Aerosol, 'Auto' for Mid-Latitude (automatic cirrus correction), 40 km visibility (default), and altitude set to 300 m (mean altitude of the target area) as inputs. The process generated atmosphere-corrected products at 60 m, 20 m, and 10 m resolutions.

Resampling and vegetation indices generation. For all bands involved in the indices or band math computation, low resolution raster data layers were resampled from 60 m and 20 m to the highest possible resolution (10 m) using the SNAP resampling processor to allow band combination.

A spectral or vegetation index is generated by combining data from multiple spectral bands into a single value. The detailed formula as well as the sources of spectral indices used in this study were shown in Table 2. The spectral indices were calculated using Sentinels Application Platform (SNAP version 6.0.5) algorithm for automatic radiometric index processing. In some equations, resampling was done to produce same band resolution. All spectral indices auto-generated using the SNAP were computed using 1.0 factor value for each band in each equation.

Table 2. Spectral indices assessed for correlation with disease severity indices (DSI) of bacterial leaf blight (BLB) from paddy fields surveyed in Cianjur, West Java, Indonesia

Indices[a]	**SNAP index processor and Band Math formula using Sentinel-2A bands**[b]	**References**
NDVI	(B8–B4)/(B8+B4)	Rouse et al. (1974)
SAVI	(1+L)*(B8–B4)/(B8+B4+L), where L is a canopy background adjustment factor	Huete (1988)
MSAVI 1	(1+L)*(B8–B4)/(B8+B4+L) where: L = 1–2*s*NDVI*WDVI, and s is the soil line slope	Qi et al. (1994)
MSAVI 2	(1/2)*(2*(B8+1)–sqrt[(2*B8+1)*(2*B8+1)–8*(B8–B4)]	Qi et al. (1994)
DVI	B8–B4	Richardson and Wiegand (1977)
RVI	R795/R675 or B8/B4	Major et al. (1990); ESA (2018)
PVI	sin(a)*B8–cos(a)*B4	Richardson and Wiegand (1977)
IPVI	B8/(B8+B4)	Crippen (1990)
WDVI	B8–g*B4	Clevers (1988)
TNDVI	sqrt[(B8–B4)/(B8+B4)+0.5]	Senseman et al. (1996)
GNDVI	(B8–B3)/(B8+B3)	Gitelson et al. (1996)
GEMI	eta*(1–0.25*eta)–(B4–0.125)/(1–B4), where, eta = (2*(B8*B8–B4*B4)+1.5*B8+0.5*B4)/(B8+B4+0.5)	Pinty and Verstraete (1992)
ARVI	(B8–rb)/(B8+rb), where rb=(B4)–gamma*(B2–B4), with gamma=1	Kaufman and Tanre (1992)
NDI45	(B5–B4)/(B5+B4)	Delegido et al. (2011)
MTCI	(B6–B5)/(B5–B4)	Dash and Curran (2004)
MCARI	[(B5–B4)–0.2*(B5–B3)]*(B5–B4)	Daughtry et al. (2000)
REIP	700+40*[(B4+B7)/2–B5]/(B6–B5)	Guyot and Baret (1988)
S2REP	705+35*[(B4+B7)/2–B5]/(B6–B5)	Guyot and Baret (1988)
IRECI	(B7–B4)/(B5/B6)	Guyot and Baret (1988)
PSSRa	B7/B4	Blackburn (1998)
SR8A4	B8A/B4	Jordan (1969)
GRE	Green*Red Edge or B3*B5	Hongo et al. (2017)
HI	[(R543–R698)/(R534+R698)]–½(R704) or (B3–B5)/(B3+B5)–½(B5)	Mahlein et al. (2012)
DWSI1	R800/R1660 or B8/B11	Apan et al. (2004)
DWSI5	(R800+R550)/(R1660+R680) or (B8+B3)/(B11+B4)	Apan et al. (2004)
CLSI	(B4–B3)/(B4+B3)–B6	Mahlein et al. (2012)
BLB1	(B8A+B3)/(B12+B4)	This study
BLB2	B11/B4	This study

[a] NDVI = Normalized Difference Vegetation Index; SAVI = Soil Adjusted Vegetation Index; MSAVI = Modified Soil Adjusted Vegetation Index; MSAVI = second Modified Soil Adjusted Vegetation Index; DVI = Difference Vegetation Index; RVI = Ratio Vegetation Index – RVI; PVI = Perpendicular Vegetation Index; IPVI = Infrared Percentage Vegetation Index; WDVI = Weighted Difference Vegetation Index; TNDVI = Transformed Normalized Difference Vegetation Index; GNDVI = Green Normalized Difference Vegetation Index; GEMI =

Global Environmental Monitoring Index; ARVI = Atmospherically Resistant Vegetation Index; NDI45 = Normalized Difference Index; MTCI = Meris Terrestrial Chlorophyll Index; MCARI = Modified Chlorophyll Absorption Ratio Index; REIP = Red-Edge Inflection Point Index; S2REP = Sentinel-2 Red-Edge Position Index; IRECI = Inverted Red-Edge Chlorophyll Index; PSSRa = Pigment Specific Simple Ratio (chlorophyll index); SR8A4 = Simple Ratio Band 8A*Band4; GRE = Green Red Edge index; DWSI = Disease and Water Stress Index; HI = Health Index; CLSI = Cercospora leaf spot index; BLB = Bacterial leaf blight index

[b] Characteristics of Sentinel-2A bands (B4, B5, B6, B,7, B8, and B8A) are shown in Table S1, and R is reflectance wavelength (nm)

Extraction of surface reflectance values from sample points (coordinates). The ArcMap (version 10.5, ESRI, California, USA) was used for viewing the satellite images and extracting geospatial data. Surface reflectance from Sentinel-2A bands acquired 24 July, 2017 and 27 September, 2018 were extracted to points or GPS coordinates of sampled rice-hills in paddy fields.

Statistical data analyses. Statistical analyses were conducted using JMP version 13 (SAS Institute, USA) and R software version 3.5.1 (R Foundation, Austria). Spearman's rank correlation was used for determining the strength of relationship between BLB severity scores per rice-hill and reflectance values of the Sentinel-2A bands which derived spectral indices. Pearson's correlation, on other hand, was used to analyse the relationship between means of BLB severity index (DSI) per plot and reflectance values of the Sentinel-2A bands which derived spectral indices. Analyses of variance (ANOVA) followed by multiple comparisons between treatments using the Tukey's Honestly Significant Difference (HSD) test was performed to determine the sensitivity of Sentinel-2A bands or sensors and the spectral indices to discriminate the different levels of BLB severity. To simplify the analysis, DSI values from sampled plots were grouped as I , initial (DSI < 25%); L, low (DSI = 25 to 49); M, moderate (DSI = 50 to 74%); and S, severe (DSI = 75 to 100%).

RESULTS AND DISCUSSION

Field assessments. A total of 22 paddy fields were assessed in six locations in 2017 whereas 30 paddy fields were assessed in four locations in 2018. In 2017, recorded BLB severity scores of sampled rice-hills ranged from 0 to 7 with highest frequency recorded at score of 5 (Fig. 2). In 2018, BLB score of 1 had the highest frequency and recorded scores ranged from 1 to 7 (Fig. 2). In general, disease severity of BLB was lower in 2018 than in 2017 because most of the rice fields surveyed in 2017 were at ripening phase whereas rice fields surveyed in 2018 varied from flowering to ripening stages. Rice plants showed severe symptoms towards maturity as more leaves became infected.

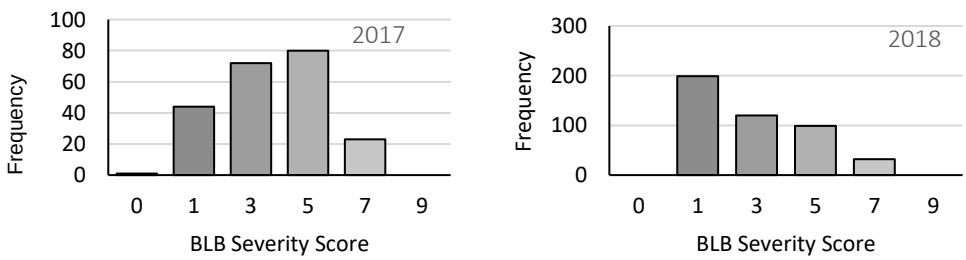

Fig. 2. Frequency distribution of BLB severity scores of each sampled rice-hill in 2017 and 2018 field assessments conducted in Cianjur, West Java, Indonesia.

Relationship between surface reflectance values of Sentinel 2-A bands and BLB severity. Correlation analyses revealed that all the bands of Sentinel-2A, except Band 10, had significant correlation with BLB disease severity gradient (Table 3). Band 4 (red, 665 nm) was the most relevant and had the strongest correlation coefficient of 0.81 with the mean DSI of 10-hill plot in 2017. In 2018,

however, Band 5 (red edge, 705 nm) was the most relevant to BLB gradient with correlation coefficient of 0.72 and 0.84 for 3-hills and 15-hills DSI means, respectively (Table 3). Band 4 (red) and Band 3 (green) also had strong correlation with BLB whereas the correlation between Band 6 (red edge, 740 nm) and BLB gradient was moderate in 2017, and weak in 2018. Band 1 (443 nm) which is designed for sensing shallow water habitat had the weakest correlation with BLB gradient in 2018. Reflectance values in the visible region (Bands 1 to 5) and shortwave infrared region (Bands 11 and 12) tended to increase as BLB severity increases, whereas values at the red edge region (Bands 6 and 7) and near-infrared region (Bands 8, 8A, and 9) tended to show the opposite movement (Table 3).

Table 3. Correlation between surface reflectance values of Sentinel 2-A bands and disease severity indices (DSI) of bacterial leaf blight (BLB) in paddy fields (2017 and 2018, Cianjur, West Java, Indonesia)

Sentinel-2A Bands	2017 DS score per hill[a]	2017 Mean DSI of 10 adjacent hills[b]	2018 Mean DSI of 3 adjacent hills[c]	2018 Mean DSI of 15 adjacent hills[d]
1	0.57**[e]	0.75**	0.26**	0.31[ns]
2	0.55**	0.76**	0.54**	0.65**
3	0.56**	0.72**	0.67**	0.81**
4	0.64**	0.81**	0.65**	0.78**
5	0.58**	0.70**	0.72**	0.84**
6	-0.43**	-0.63**	-0.34**	-0.42*
7	-0.52**	-0.73**	-0.51**	-0.62**
8	-0.52**	-0.70**	-0.47**	-0.57 **
8A	-0.50**	-0.71**	-0.45**	-0.56**
9	-0.58**	-0.80**	-0.48**	-0.56**
10	n/a[f]	n/a	n/a	n/a
11	0.61**	0.67**	0.33**	0.45*
12	0.64**	0.72**	0.43**	0.56**

[a] Correlation coefficient values from Spearman's rank correlation between BLB disease severity scores per rice-hill and the Sentinel-2A bands' reflectance values (satellite image acquired on July 24, 2017)

[b] Correlation coefficient values from Pearson's correlation between BLB disease severity index per plot of 10 adjacent rice-hills sampled across a rice paddy field (10m – 20 m across) and the Sentinel-2A bands' reflectance values (satellite image acquired on July 24, 2017). Disease severity index (DSI) = Σ[(number of rice-hills at the scale)/(10 hills×9)]×100

[c] Correlation coefficient values from Pearson's correlation between BLB disease severity index per plot of 3 adjacent rice-hills sampled within a $1m^2$ area and the Sentinel-2A bands' reflectance values (satellite image acquired on Sept. 27, 2018). Disease severity index (DSI) = Σ[(number of rice-hills at the scale)/(3 hills×9)] ×100

[d] Correlation coefficient values from Pearson's correlation between mean BLB disease severity index of 15 adjacent rice-hills from 5 sampled plots within the same paddy field and the Sentinel-2A bands' reflectance values (satellite image acquired on Sept. 27, 2018). Disease severity index (DSI) = Σ[(number of rice-hills at the scale)/(15 hills×9)]×100

[e] Notation for the probability level (*p*-value) for the analysis of variance: ** for $p<0.01$; * for $p<0.05$ and [ns] for $p>0.05$

[f] n/a, not applicable. Band 10 was excluded since reflectance values were used in cirrus cloud correction

This is the first study that attempted to utilize Sentinel-2 satellite data to differentiate various levels of BLB severity. Sentinel-2 satellite data are freely accessible while satellite products of LISS IV and RapidEye used in previous studies (Das et al. 2015; Hongo et al. 2017) are not free. Moreover, Sentinel-2 has visible (VIS) and near-infrared (NIR) bands with 10 m spatial resolution which is higher than other free access satellite products such as Landsat 8 of NASA/USGS with 30 m resolution for visible and NIR regions and 15 m for panchromatic band. Overall, correlation coefficients between BLB severities and Sentinel-2A bands were higher when the means of DSI in 2017 and in 2018 were fitted against the means of the reflectance values.

In terms of band sensitivity to discriminate BLB severity, Bands 1 (coastal aerosol), 2 (blue), 3 (green), 4 (red) and 5 (red edge) of the visible region of spectrum significantly separated the severity ranks. Shortwave infrared regions covered by Bands 11 and 12 also significantly separated the severe BLB from low and moderate disease severities (Table 4). Our results agree with Apan et al. (2004) indicating that incorporation of SWIR band (1660 nm) in disease indices provided the maximum discrimination between disease and non-diseased sugarcane plants. Vegetative red edge region (Bands 6 and 7) and NIR (Bands 8 and 8A) were moderately sensitive in discriminating severe from moderate level but could still be relevant and significantly separate initial and low levels of BLB severity from more severe cases.

Table 4. Sensitivity of Sentinel-2A bands to disease severity indices (DSI) of bacterial leaf blight (BLB) in paddy fields [a].

Sentinel-2A Bands	F[b]	p-value[b]	Level of BLB severity[c]			
			I	L	M	S
1	44.01	<0.001	7.73[a]	8.27[b]	8.50[c]	8.89[d]
2	42.97	<0.001	7.16[a]	7.62[b]	7.88[c]	8.20[d]
3	38.54	<0.001	9.03[a]	9.48[b]	9.74[c]	10.11[d]
4	55.44	<0.001	7.10[a]	8.09[b]	8.60[c]	9.17[d]
5	37.82	<0.001	11.71[a]	12.46[b]	12.89[c]	13.58[d]
6	33.98	<0.001	22.50[a]	21.22[b]	20.96[b]	21.11[b]
7	54.79	<0.001	27.20[a]	24.93[b]	24.36[c]	24.55[bc]
8	40.46	<0.001	26.50[a]	24.64[b]	23.98[c]	24.17[bc]
8A	45.41	<0.001	29.35[a]	27.19[b]	26.60[c]	26.72[bc]
9	77.50	<0.001	25.60[a]	23.58[b]	22.95[c]	22.82[c]
11	34.30	<0.001	15.89[a]	16.69[b]	17.21[c]	18.68[d]
12	39.00	<0.001	8.83[a]	9.77[b]	10.31[c]	11.44[d]

[a] Reflectance values were extracted from atmosphere-corrected Sentinel-2 imagery obtained on 24 July, 2017 covering the Cianjur, West Java, Indonesia site

[b] F statistic and p-value obtained from the analysis of variance (ANOVA)

[c] Mean comparison of DSI levels of BLB according to Tukey's HSD. Means with same letter in each row are not significantly different at $p<0.05$. Levels of DSI per rice-hill are described as I – initial (DSI < 25), L – low (DSI = 25 to 49); M – moderate (DSI = 50 to 74), and S – severe (DSI = 75 to 100)

Surface reflectance difference between BLB infected and healthy rice plants at canopy level measurements was high at green and red edge regions. In general, BLB infection on mature rice plants results in chlorosis as an initial symptom (Hongo et al. 2017). As infection advances, lesions form, and leaves start to turn brown and eventually wilt. Many studies indicated that visible region particularly the green, in addition to red edge, near-infrared and shortwave or mid-infrared regions may be relevant as these regions represent physiological change in plants (Caasi et al. 2019; Calderon et al. 2013; Knipling 1970; Mirik et al. 2011; Reynolds et al. 2012). Reflectance values at the NIR region are usually higher than the other regions because of internal leaf scattering and no light absorption, whereas plant leaf typically has a low reflectance in the visible spectral region because of strong absorption by chlorophylls (Knipling 1970). There is a relatively low reflectance in the infrared beyond 1,300 nm because of strong absorption by water. When the chlorophyll content of infected plants decreases, higher reflectance is observed in the visible green and red edge regions (Calderon et al. 2015; Knipling 1970; Mirik et al. 2011). On the other hand, infected or stressed plants usually show lower spectral reflectance in the NIR region as leaf structure is altered and canopy density, biomass and leaf area decrease (Calderon et al. 2013; Knipling 1970). Changes in middle-infrared reflectance region in water-stressed sugar beet foliage was due to mixture of vegetation and soil background reflectance as the canopy of plants start to collapse (Reynolds et al. 2012). The highest separability between diseased and non-diseased sugarcane was in the NIR region (between 750 to 880 nm and 1070 nm) and followed by selected ranges in the SWIR particularly at 1660 nm and 2200 nm, green (550 nm) and red (680 nm)

regions (Apan et al. 2004). There is good correlation between BLB disease intensity and spectral reflectance from 325 to 1075 nm (Singh et al. 2012). Hyperspectral canopy reflectance measurement of BLB-infected rice cultivars by Yang (2010) showed that for moderately susceptible rice cultivars, 757 to 1039 nm were the most sensitive region of spectrum to BLB, whereas for highly susceptible cultivars, all the narrow bands are relevant.

Relationship between spectral indices from Sentinel-2A bands and BLB severity. Most of the spectral indices exhibited highly significant correlations with BLB severity gradients except for Modified Chlorophyll Absorption Ratio Index (MCARI) in 2018 field surveys (Table 5). It is also noted that most of the spectral indices showed downward trend as the BLB severity increased, whereas Cercospora leaf spot index (CLSI) and Green Red Edge Index formula 1 (GRE) showed an upward trend (Table 5). Pigment Specific Simple Ratio chlorophyll-*a* (PSSRa), Ratio Vegetation Index (RVI), Simple Ratio (SR8A4) had the highest correlation with BLB severity gradient per 10-hill plot (r = -0.84, p<0.01) in 2017 field survey (Table 5). Other spectral indices also showed highly significant (p<0.01) correlation with BLB severity gradient (mean DSI per 10-hill plot) such as Atmospherically Resistant Vegetation Index (ARVI, r = -0.83), Normalized Difference Index (NDI45, r = -0.83), Inverted Red-Edge Chlorophyll Index (IRECI, r = -0.83), Normalized Difference Vegetation Index (NDVI, r = -0.82), Infrared Percentage Vegetation Index (IPVI, r = -0.82), and Transformed Normalized Difference Vegetation Index (TNDVI, r = -0.82). Soil Adjusted Vegetation Index (SAVI), Difference Vegetation Index, Green Normalized Difference Vegetation Index (GNDVI), Modified Soil Adjusted Vegetation Index (MSAVI), Second Modified Soil Adjusted Vegetation Index (MSAVI2) were also highly correlated to BLB severity (Table 5). In 2018 field survey (15-hill DSI), the highest correlation was found with Meris Terrestrial Chlorophyll Index (MTCI) (r = -0.84) followed by GRE (r = 0.83).

Health index (HI), an index for detecting sugar beet foliar disease, had the strongest correlation with BLB severity gradient with a coefficient of -0.84 in 2018 (15-hill DSI) (Table 5). However, the correlation was lower in 2017 with a coefficient of -0.70 (10-hill DSI). In 2017, the Bacterial Leaf Blight index 1 (BLB1) proposed in this study had the strongest correlation with BLB severity gradient per 10-hill plot with r = -0.83 followed by Disease-Water Stress Index formula 5 with -0.82. BLB index 2, on the other hand, had strong correlation with the BLB severity of 2018 with r = -0.81. DWSI 1 had moderate correlation with BLB (10-hill DSI) with r = -0.79 in 2017 and r = -0.62 in 2018 (15-hill DSI).

Table 5. Correlation between spectral indices from Sentinel-2A bands and disease severity indices (DSI) of bacterial leaf blight (BLB) in paddy fields (2017 and 2018, Cianjur, West Java, Indonesia).

Spectral Index[a]	2017 DS Score per hill[b]	2017 Mean DSI per 10 adjacent hills[c]	2018 Mean DSI of 3 adjacent hills[d]	2018 Mean DSI of 15 adjacent hills[e]
NDVI	-0.66** [f]	-0.82**	-0.61**	-0.74**
ARVI	-0.67**	-0.83**	-0.65**	-0.78**
DVI	-0.62**	-0.80**	-0.54**	-0.65**
GEMI	-0.60**	-0.79**	-0.52**	-0.63**
GNDVI	-0.62**	-0.81**	-0.62**	-0.74**
IPVI	-0.66**	-0.82**	-0.61**	-0.74**
IRECI	-0.62**	-0.83**	-0.63**	-0.74**
MCARI	-0.51**	-0.76**	0.11[ns]	0.17[ns]
MSAVI	-0.64**	-0.81**	-0.56**	-0.67**
MSAVI2	-0.64**	-0.81**	-0.56**	-0.68**
MTCI	-0.53**	-0.76**	-0.69**	-0.84**
NDI45	-0.62**	-0.83**	-0.43**	-0.55**
PSSRa	-0.65**	-0.84**	-0.64**	-0.76**
REIP	-0.44**	-0.64**	-0.67**	0.65**
RVI	-0.66**	-0.84**	-0.63**	-0.80**

Spectral Index[a]	2017 DS Score per hill[b]	2017 Mean DSI per 10 adjacent hills[c]	2018 Mean DSI of 3 adjacent hills[d]	2018 Mean DSI of 15 adjacent hills[e]
S2REP	-0.44**	-0.64**	-0.67**	-0.80**
SAVI	-0.64**	-0.81**	-0.56 **	0.68**
TNDVI	-0.66**	-0.82**	-0.61**	-0.73**
WDVI	-0.58**	-0.77**	-0.51**	-0.61**
SR8A4	-0.65**	-0.84**	-0.63**	-0.74**
GRE	0.57**	0.71**	0.70**	0.83**
HI	-0.58**	-0.70**	-0.72**	-0.84**
CLSI	0.44**	0.64**	0.35**	0.44*
DWSI1	-0.65**	-0.79**	-0.55**	-0.62**
DWSI5	-0.66**	-0.82**	-0.55**	-0.66**
BLB1	-0.65**	-0.83**	-0.57**	-0.69**
BLB2	-0.46**	-0.68**	-0.69**	-0.81**

[a] Sources and formula of spectral indices were shown in Table S2

[b] Correlation coefficient values from Spearman's rank correlation between BLB scores of rice-hills and the reflectance values of Sentinel-2A bands (satellite image acquired on 24 July, 2017)

[c] Correlation coefficient values from Pearson's correlation between BLB severity index per plot of 10 adjacent rice-hills sampled across a rice paddy field (10m – 20 m across) and the Sentinel-2A bands' reflectance values (satellite image acquired on 24 July, 2017). Disease severity index (DSI)=Σ[(number of rice-hills at the scale)/(10 hills×9)]×100

[d] Correlation coefficient values from Pearson's correlation between BLB severity index per plot of 3 adjacent rice-hills sampled within a 1 m^2 area and the Sentinel-2A bands' reflectance values (satellite image acquired on Sept. 27, 2018). Disease severity index (DSI)=Σ[(number of rice-hills at the scale)/(3 hills×9)]×100

[e] Correlation coefficient values from Pearson's correlation between mean BLB severity index of 15 adjacent rice-hills from 5 sampled plots within the same paddy field and the Sentinel-2A bands' reflectance values (satellite image acquired on 27 September, 2018). Disease severity index (DSI)=Σ[(number of rice-hills at the scale)/(15 hills×9)]×100

[f] Notation for the probability level (*p*-value) for the analysis of variance: ** for $p<0.01$; * for $p<0.05$; and ns for $p>0.05$

Among the spectral indices, DWSI1, DWSI5, GRE and BLB1, were very sensitive and had significantly discriminated all the levels of BLB severity ($p<0.05$) (Table 6). Other spectral indices were less sensitive in separating the BLB severity levels as no significant differences were observed between the severe and moderate levels (Table 6). Nonetheless, most of these indices, except MCARI, could still be used to discriminate moderate and severe symptoms from lower levels.

Table 6. Sensitivity of spectral indices from the Sentinel-2 bands to the disease severity indices (DSI) of bacterial leaf blight (BLB) in paddy fields.

Spectral index[a]	*F*[b]	*p*-value[b]	DSI levels of BLB per rice-hill[c]			
			I	L	M	S
NDVI	59.74	<0.001	0.58^{a}	0.51^{b}	0.47^{c}	0.45^{c}
ARVI	57.66	<0.001	0.58^{a}	0.49^{b}	0.44^{c}	0.42^{c}
DVI	58.88	<0.001	0.19^{a}	0.17^{b}	0.15^{c}	0.15^{c}
GEMI	56.88	<0.001	0.66^{a}	0.61^{b}	0.60^{c}	0.59^{c}
GNDVI	60.52	<0.001	0.50^{a}	0.45^{b}	0.43^{c}	0.42^{c}
IPVI	59.34	<0.001	0.79^{a}	0.75^{b}	0.74^{c}	0.73^{c}
IRECI	72.46	<0.001	0.39^{a}	0.29^{b}	0.26^{c}	0.24^{c}
MCARI	23.16	<0.001	0.07^{a}	0.06^{b}	0.05^{c}	0.05^{bc}
MSAVI	60.80	<0.001	0.30^{a}	0.26^{b}	0.24^{c}	0.23^{c}
MSAVI2	61.98	<0.001	0.82^{a}	0.77^{b}	0.75^{c}	0.74^{c}
MTCI	24.12	<0.001	2.36^{a}	2.01^{b}	1.95^{b}	1.72^{c}
NDI45	37.91	<0.001	0.25^{a}	0.21^{b}	0.20^{c}	0.19^{c}

Spectral index[a]	F[b]	p-value[b]	DSI levels of BLB per rice-hill[c]			
			I	L	M	S
PSSRa	74.56	<0.001	3.86[a]	3.13[b]	2.86[c]	2.70[c]
REIP	17.52	<0.001	720.14[a]	718.24[b]	717.83[b]	717.64[b]
RVI	71.27	<0.001	3.16[a]	3.10[b]	2.81[c]	2.67[c]
S2REP	17.52	<0.001	722.63[a]	720.96[b]	720.60[b]	720.44[b]
SAVI	60.34	<0.001	0.35[a]	0.30[b]	0.28[c]	0.27[c]
TNDVI	57.46	<0.001	1.04[a]	1.00[b]	0.99[c]	0.98[c]
WDVI	52.45	<0.001	0.23[a]	0.21[b]	0.20[c]	0.20[c]
SR8A4	74.10	<0.001	3.76[a]	3.09[b]	2.81[c]	2.65[c]
GRE	38.55	<0.001	105.92[a]	118.47[b]	125.91[c]	137.54[d]
HI	37.50	<0.001	-11.38[a]	-10.74[b]	-10.62[c]	-10.70[c]
CLS1	35.53	<0.001	-22.62[a]	-21.30[b]	-21.02[c]	-21.16[c]
DWSI1	53.46	<0.001	1.67[a]	1.48[b]	1.40[c]	1.30[d]
DWSI2	6.70	<0.001	1.76[a]	1.76[b]	1.77[b]	1.85[b]
DWSI5	60.77	<0.001	1.55 [a]	1.38 [b]	1.31 [c]	1.24 [d]
BLB1	66.98	<0.001	2.42[a]	2.07[b]	1.94[c]	1.80[d]
BLB2	21.68	<0.001	0.98[a]	1.03[b]	1.06[b]	1.13[c]

[a] Spectral indices were calculated from atmospheric corrected Sentinel-2 imagery obtained on 24 July, 2017 covering the Cianjur, West Java, Indonesia. The equation formula are shown in Table S2

[b] F statistic and p-value obtained from the analysis of variance (ANOVA)

[c] Mean comparison of DSI levels of BLB according to Tukey's HSD. Means with same letter in each row are not significantly different at $p<0.05$. Levels of DSI per rice-hill are described as I, initial (DSI < 25); L, low (DSI = 25 to 49); M, moderate (DSI = 50 to 74); and S, severe (DSI = 75 to 100)

Indices such as NDVI can be used to detect rice canopy symptoms and damage caused by various factors (Das et al. 2015; Ghobadifar et al. 2016; Hongo et al. 2015; Mirik et al. 2011; Singh et al. 2012). For example, changes in canopy density due to infection causes reduction in leaf reflectance at NIR, hence decreases the NDVI value of a certain vegetation. Indices such as Pigment Specific Simple Ratio (PSSRa and PSSRb), on the other hand, can detect anomalies in the chlorophyll content of plants due to infection (Calderon et al. 2013; Das et al. 2015). Plant with chlorosis for example would tend to increase in PSSR index value as chlorophyll content decreases since reflectance values at RGB region tend to increase when leaf chlorophyll abundance is low as more light is reflected than absorbed (Calderon et al. 2013; Das et al. 2015). Vegetation indices such as NDVI, SR (Simple Ratio), red edge, and OSAVI (optimized soil-adjusted vegetation index) were highly correlated to BLB severities on rice (Singh et al. 2012).

The strong correlation between BLB severity and most of the spectral indices tested in this study such as NDVI, RVI, and ARVI showed the consistency of these indices as structural damage and canopy density indicators. The usefulness of structural indices as indicator of Verticillium wilt damage on olive trees (Calderon et al. 2013). Chlorophyll content indices such as PSSRa and GRE also showed consistency because of their sensitivity to changes in chlorophyll content of the leaves affected by BLB.

The four highly relevant spectral indices, DWSI1, DWSI5, GRE and BLB1 were laid over the ESRI ArcGIS map of paddy fields in Sukatani, Cianjur, West Java, Indonesia, generating geo-spatial maps to exhibit the BLB severity across a wide swath of land (Fig. 3). In addition, two other common spectral indices, NDVI and RVI, were also used to create their GIS maps for comparison. All these spectral indices showed variation in the BLB severities, indicating their potential usability to estimate BLB severity. However, BLB1, DWSI1, DWSI5, NDVI, and RVI exhibited almost similar patterns of the disease severity, whereas the GRE index map showed a different pattern.

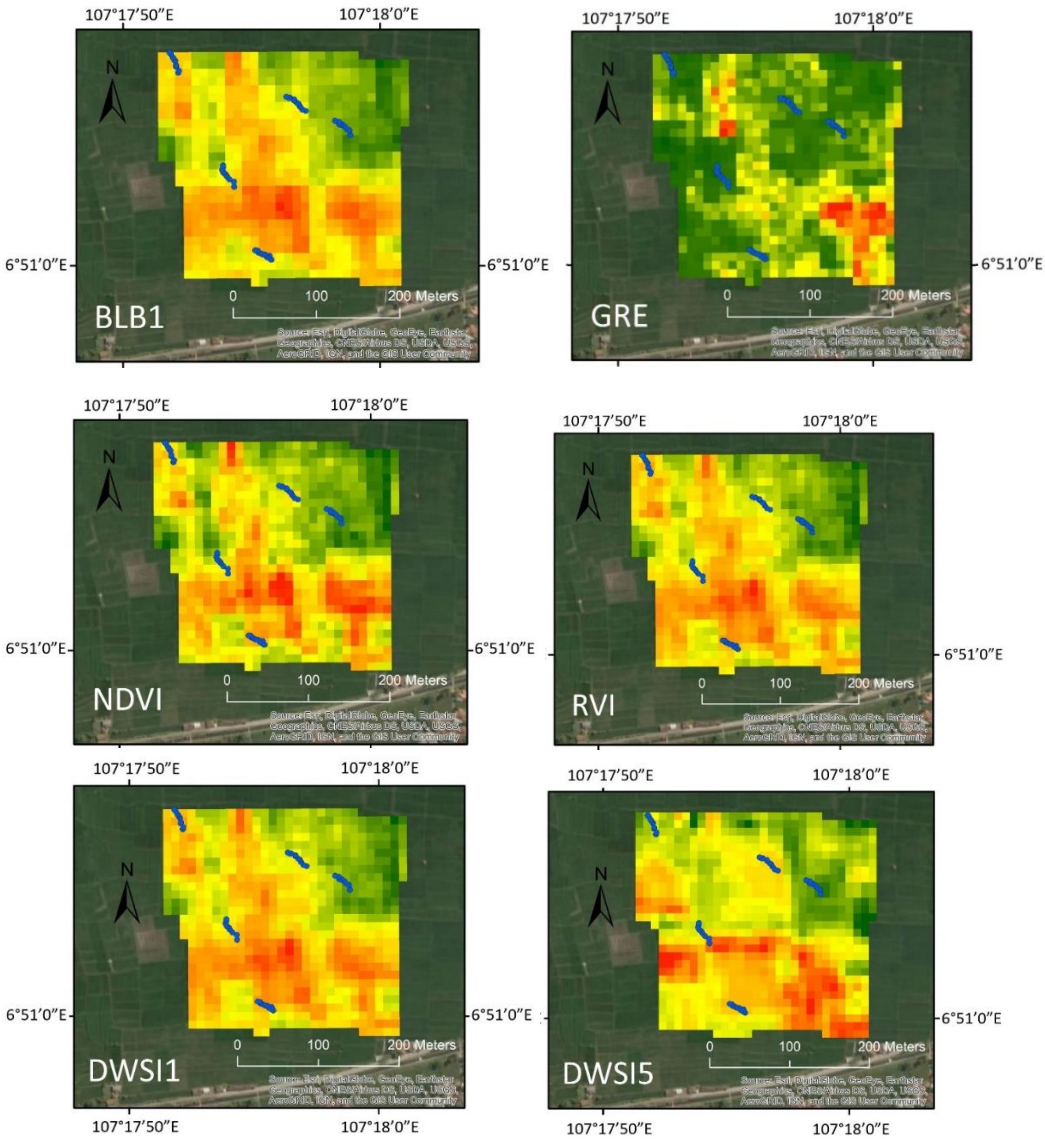

Fig. 3. GIS maps generated using BLB Index 1 (BLB1), Green Red Edge (GRE) index, Normalized Difference Vegetation Index (NDVI), Ratio Vegetation Index (RVI), Disease and Water Stress Index 1 (DWSI1) and Disease and Water Stress Index 5 (DWSI5) at 10 m resolution laid over the ESRI ArcGIS map of rice fields in Sukatani, Cianjur, West Java, Indonesia, showing variation in the indices values which can potentially estimate BLB severity. Actual geospatial position of sample plots across rice paddy fields are shown here as blue dots.

The relationship between BLB and relative chlorophyll abundance in rice leaves in West Java was inversely correlated to SPAD values and had the highest correlation coefficient among rice diseases and pest damage observed in the field (Caasi et al. 2019). Moreover, BLB was the most dominant among the diseases observed which also included narrow brown spot, sheath blight, and rice blast and whitehead caused by stemborer. Whitehead, sheath blight and blast had low prevalence and did not affect rice chlorophyll content. Narrow brown spot appeared to be associated to severe BLB but had low correlation to chlorophyll reduction of the leaves nor the yield of the rice. In a complex rice and

disease interactions with multi-infection scenario, it is difficult to accurately estimate BLB damage on rice using multispectral data since some diseases have similar symptoms and spatial patterns. Nevertheless, for the purposes of damage assessment of rice paddies for crop insurance claim, the method developed, and the information generated in this study will help in generating GIS maps that could provide spatial pattern of damage caused by BLB that may or may not include other diseases and pest damage. In the crop insurance policy being implemented in Indonesia, claims are based on total crop area damaged and do not require identification of specific natural cause (Pasaribu 2016). Hence, this method could still have practical use in the future.

The next step would be to develop remote sensing system using hyperspectral sensors with higher spatial resolution whether from satellite system or attached to unmanned aerial vehicle or drone platforms (Yang 2010; Martinelli et al. 2015; Gogoi et al. 2018). However, the public have limited access to data from satellites with hyperspectral sensors and high spatial resolutions. Acquiring images are also expensive. UAV-based systems with multispectral or hyperspectral sensors are now currently being developed, however, commercial systems are still expensive (Yang 2010; Martinelli et al. 2015; Gogoi et al. 2018). Moreover, farmers and researchers in developing countries have limited access to hardware, software, and techniques for advance remote sensing (George 2000; Haack and Ryerson 2016).

CONCLUSION

Most of the Sentinel-2 bands and spectral indices tested in this study are relevant to BLB detection. Disease indices such as Green Red Edge (GRE) index and Disease-Water Stress indices (DWSI1 and DWSI5) were found to be the most sensitive in separating the levels of BLB severity. Bacterial Leaf Blight index formula 1 (BLB1), NDVI and RVI were also relevant and sensitive in separating severe BLB damage from other levels. Sentinel-2 satellites sensors have the potential of detecting and estimating BLB damage. With additional relevant data and more parameters, geo-spatial maps generated with relevant bands and spectral indices could provide in the future useful geospatial information of rice paddies for BLB disease management strategies as well as crop insurance policy claims.

ACKNOWLEDGEMENTS

This study was conducted as a part of the Science and Technology Research Partnership for Sustainable Development (SATREPS) program, titled “Development and implementation of new damage assessment process in agricultural insurance as adaptation to climate change for food security” funded by the Japan Science and Technology Agency (JST) and the Japan International Cooperation Agency (JICA).

REFERENCES CITED

Apan, A., Held, A., Phinn, S., and J. Markley. 2004. Detecting sugarcane ‘orange rust’ disease using EO-1 Hyperion hyperspectral imagery. Int. J. Remote Sens. 25: 489-498.

Blackburn, G.A. 1998. Spectral indices for estimating photosynthetic pigment concentrations: a test using senescent tree leaves. Int. J. Remote Sens. 19: 657-675.

Caasi, O., Hongo, C., Suryaningsih, A., Wiyono, S., Homma, K., and M. Shishido. 2019. Relationships between bacterial leaf blight and other diseases based on field assessment in Indonesia. Trop. Agric. Dev. 63: 113－121.

Calderón, M., Cortés, J., Lucena, C., and P. Zarco-Tejada. 2013. High-resolution airborne hyperspectral and thermal imagery for early detection of *Verticillium* wilt of olive using fluorescence, temperature and narrow-band spectral indices. Remote Sens. Environ. 139: 231-245.

Clevers, J. G. 1988. The derivation of a simplified reflectance model for the estimation of leaf area index. Remote Sens. Environ. 25: 53-70.

Cordova, A.F., Ramos, V.H., Irwin, D., and T. Sever. 2012. Advances in remote sensing applications for environmental management in Central America. In Proc. International Astronautical Congress, IAC Vol. 4: 2968-2980. The 63rd IAC, Naples, Italy, October 1-5, 2012.

Crippen, R. E. 1990. Calculating the vegetation index faster. Remote Sens. Environ. 34: 71-73

Das, P. K., Laxman, B., Rao, S. V., Seshasai, M. V., and V. K. Dadhwal. 2015. Monitoring of bacterial leaf blight in rice using ground-based hyperspectral and LISS IV satellite data in Kurnool, Andhra Pradesh. India. Int. J. Pest Manage. 61: 359-368.

Dash, J. and P. Curran. 2004. The MERIS terrestrial chlorophyll index. Int. J. Remote Sens. 25: 257.

Daughtry, C., Walthall, C. L., Kim, M. S., Brown de Colstoun, E., and J. E. M. III. 2000. Estimating corn leaf chlorophyll concentration from leaf and canopy reflectance. Remote Sens. Environ. 74: 229-239.

Delegido, J., Verrelst, J., Alonso, L., and J. Moreno. 2011. Evaluation of Sentinel-2 red-edge bands for empirical estimation of green LAI and chlorophyll content. Sensors 11: 7063-7081

Delp, B. R., Stowell, L. J., and J. J. Marois. 1986. Evaluation of field sampling techniques for estimation of disease incidence. Phytopathology 76: 1299-1305.

ESA [European Space Agency]. 2018. Step: Science toolbox exploitation platform. SNAP: Sentinel Application Platform. http://step.esa.int/main/toolboxes/snap/ (browsed on April 10, 2018).

ESA [European Space Agency]. 2019. Sentinel Online. https://earth.esa.int/web/sentinel/technical-guides/sentinel-2-msi/msi-instrument (browsed on May 1, 2019).

FAO [Food and Agriculture Organization of the United Nations]. 2019. Pro-poor policy options: The case for rice crop insurance in Indonesia. Retrieved from: https://fao.org/3/a-bo568e.pdf

George, H. 2000. Developing countries and remote sensing: how intergovernmental factors impede progress. Space Policy 16: 267-273.

Ghobadifar, F., Aimrun, W., and M.N. Jebur. 2016. Development of an early warning system for brown planthopper (BPH) (*Nilaparvata lugens*) in rice farming using multispectral remote sensing. Precis. Agric. 17: 377-391.

Gitelson, A. A., Kaufman, Y. J., and M. N. Merzlyak. 1996. Use of a green channel in remote sensing of global vegetation from EOS-MODIS. Remote Sens. Environ. 58: 289-298.

Gogoi, N. K., Deka, B., and L.C. Bora. 2018. Remote sensing and its use in detection and monitoring plant diseases: A review. Agric. Rev. 10: 1805-1835.

Guyot, G. and F. Baret. 1988. Spectral signatures of objects in remote sensing. In Proc. 4th International Colloquium (ESA) Paris, pp. 279-286.

Haack, B. and R. Ryerson. 2016. Improving remote sensing research and education in developing countries: Approaches and recommendations. Int. J. Appl. Earth Obs. Geoinf. 45: 77-83.

Hongo, C., Takahashi, Y., Sigit, G., and E. Tamura. 2017. Evaluation of bacterial leaf blight of rice using hyperspectral data. In Proc. 7th Asian-Australasian Conference on Precision Agriculture. Hamilton, New Zealand October 16-18, 2017.

Hongo, C., Tsuzawa, T., Tokui, K., and E. Tamura. 2015. Development of damage assessment method of rice crop for agricultural insurance using satellite data. J. Agric. Sci. 7: 12.

Huete, A. 1988. A soil-adjusted vegetation index (SAVI). Remote Sens. Environ. 25: 295-309.

IRRI [International Rice Research Institute]. 2017. Bacterial leaf blight. IRRI Rice Knowledge Bank. http://www.knowledgebank.irri.org/decision-tools/rice-doctor/rice-doctor-fact-sheets/item/bacterial-blight (browsed on July 27, 2017).

Jordan, C. F. 1969. Derivation of leaf area index from quality of light on the forest floor. Ecology 50: 663-666.

Kaufman, J. Y. and D. Tanre. 1992. Atmospherically resistant vegetation index (ARVI) for EOS-MODIS. Geoscience and Remote Sensing, IEEE Trans. Geosci. Remote Sens. 30: 261-270.

Knipling, E. 1970. Physical and physiological basis for the reflectance of visible and near-infrared radiation from vegetation. Remote Sens. Environ. 1: 155-159.

Louis, J., Debaecker, V., Pflug, B., Main-Knorn, M., Bieniarz, J., Müller-Wilm, U., Cadau, E., and F. Gascon. 2016. Sentinel-2 Sen2cor: L2A Processor for Users. In Proc. Living Planet Symposium 2016. Prague, Czech Republic May 9-13, 2016.

Mahlein, A. K., Rumpf, T., Welke, P., Dehne, H. W., Plümer, L., Steiner, U., and E. C. Oerke. 2013. Development of spectral indices for detecting and identifying plant diseases. Remote Sens. Environ. 128: 21-30.

Major, D. J., Baret, F., and G. Guyot. 1990. A ratio vegetation index adjusted for soil brightness, Int. J. Remote Sens. 11(5): 727-740.

Martinelli, F., Scalenghe, R., and S. Davino. 2015. Advanced methods of plant disease detection. A review. Agron. Sustain. Dev. 35 (1): 1-25.

Mew, T. W., Alvarez, A. M., Leach, J. E., and J. Swings. 1993. Focus on bacterial blight of rice. Plant Dis. 77: 5-12.

Mirik, M., Jones, D. C., Price, J. A., Workneh, F., Ansley, R. J., and C. M. Rush. 2011. Satellite remote sensing of wheat infected by Wheat streak mosaic virus. Plant Dis. 95: 4-12.

Pasaribu, S. M. 2010. Developing rice farm insurance in Indonesia. Agriculture and Agricultural Science Procedia 1, 33 – 41. International Conference on Agricultural Risk and Food Security 2010.

Pasaribu, S. M. 2016. Implementation of indemnity-based rice crop insurance in Indonesia. The Food and Fertilizer Technology Center (FFTC). FFTC Agricultural Policy Articles. Retrieved from: http://ap.fftc.agnet.org/ap_db.php?id=650

Pinty, B. and M. Verstraete. 1992. GEMI: A non-linear index to monitor global vegetation from satellites. Vegetatio. 101: 15-20.

Qi, J., Chehbouni, A., Huete, A., Kerr, Y. H., and S. Sorooshian. 1994. A modified soil adjusted vegetation index. Remote Sens. Environ. 48: 119-126.

Reitsma, J. and P. Schure. 1950. *Kresek*, a bacterial disease of rice. Contributions from the General Agricultural Research Station, Bogor 117: 17.

Reynolds, G. J., Windels, C. E., MacRae, I. V., and S. Laguette. 2012. Remote sensing for assessing Rhizoctonia crown and root rot severity in sugar beet. Plant Dis. 96: 497-505.

Richardson, A. J. and C.L. Wiegand. 1977. Distinguishing vegetation from soil background information. Photogramm. Eng. Remote Sens. 43: 1541-1552.

Rouse, J.W., Haas, R. H., Schell, J. A., and D.W. Deering. 1974. Monitoring vegetation systems in the Great Plains with ERTS. In S.C. Freden, E.P. Mercanti, and M. Becker (eds.). Third Earth Resources Technology Satellite-1 Symposium. Volume I: Technical Presentations. NASA, Washington, D.C. pp. 309-317.

Senseman, G.M., Bagley, C. F., and S.A. Tweddale. 1996. Correlation of rangeland cover measures to satellite-imagery-derived vegetation indices, Geocarto Int. 11: 29-38.

Singh, B., Singh, M., Singh, G., Suri, K., Pannu, P., and S.K. Bal. 2012. Hyper-spectral data for the detection of rice bacterial leaf blight (BLB) disease. In Proc. Agro-Informatics and Precision Agriculture (AIPA): The Third National Conference. August 1-3, 2012.

Swings, J., Van Den Mooter, M., Vauterin, L., Hoste, B., Gillis, M., and T.W. Mew. 1990. Reclassification of the causal agents of bacterial blight (*Xanthomonas campestris* pv. *oryzae*) and bacterial leaf streak (*Xanthomonas campestris* pv. *oryzicola*) of rice as pathovars of *Xanthomonas oryzae* (ex Ishiyama 1922) sp. nov., nom. rev. Int. J. Syst. Bacteriol. 40: 309-311.

USGS [United States Geological Survey]. 2018. Earth Explorer Platform. https://earthexplorer.usgs.gov/ (Accessed on October 13, 2018).

Yang, C. M. 2010. Assessment of the severity of bacterial leaf blight in rice using canopy hyperspectral reflectance. Precis. Agric. 11: 61-81.